



# The application of weighted gene co-expression network analysis in identifying key modules and hub genes associated with disease status in Alzheimer's disease

Yan Sun, Jinghan Lin, Liming Zhang

Department of Neurology, The First Affiliated Hospital of Harbin Medical University, Harbin 150000, China

**Contributions:** (I) Conception and design: L Zhang; (II) Administrative support: Y Sun, J Lin; (III) Provision of study materials or patients: Y Sun; (IV) Collection and assembly of data: Y Sun, J Lin; (V) Data analysis and interpretation: All authors; (VI) Manuscript writing: All authors; (VII) Final approval of manuscript: All authors.

**Correspondence to:** Liming Zhang. Ward 4, Department of Neurology, The First Affiliated Hospital of Harbin Medical University, No. 23, Postal Street, Nangang District, Harbin 150000, China. Email: zfx0001@126.com.

**Background:** Alzheimer's disease (AD) is the most common neurodegenerative condition that affects more than 15 million individuals globally. However, a predictive molecular biomarker to distinguish the different stages of AD patients is still lacking.

**Methods:** A weighted gene co-expression network analysis (WGCNA) was employed to systematically identify the co-expressed gene modules and hub genes connected with AD development based on a microarray dataset (GSE1297) from the Gene Expression Omnibus (GEO) database. An independent validation cohort, GSE28146, was utilized to assess the diagnostic efficiency for distinguishing the different stages of AD. Quantitative real-time reverse transcription polymerase chain reaction (qRT-PCR) and western blotting analysis were applied to examine the mRNA and protein level of GRIK1, respectively, in AD mice established with the expression of mutant amyloid precursor protein and wild type mice. The morphology of neurons was investigated using phalloidin staining.

**Results:** We identified 16 co-expressed genes modules, with the pink module showing significant association with all three disease statuses [neurofibrillary tangle (NFT), BRAAK, and mini-mental state examination (MMSE)]. Enrichment analysis specified that these modules were enriched in phosphatidylinositol 3-kinase (PI3K) signaling and ion transmembrane transport. The validation cohort GSE28146 confirmed that six hub genes in the pink module could distinguish severe and non-severe AD patients [area under the curve (AUC) >0.7]. These hub genes might act as a biomarker and help to differentiate diverse pathological stages for AD patients. Finally, one of the hubs, GRIK1, was validated by an animal AD model. The mRNA and protein level of GRIK1 in the AD hippocampus was increased compared with the control group (NC) hippocampus. Phalloidin staining showed that dendritic length of the GRIK1 pCDNA3.1 group was shorter than that of the NC group.

**Conclusions:** In summary, we systematically recognized co-expressed gene modules and genes related to AD stages, which gave insight into the fundamental mechanisms of AD progression and revealed some probable targets for the treatment of AD.

**Keywords:** Alzheimer's disease (AD); weighted gene co-expression network analysis (WGCNA); pathological stage; gene modules

Submitted Aug 30, 2019. Accepted for publication Nov 26, 2019.

doi: 10.21037/atm.2019.12.59

**View this article at:** <http://dx.doi.org/10.21037/atm.2019.12.59>

## Introduction

Alzheimer's disease (AD), as the most common neurodegenerative condition, affects more than 15 million people worldwide (1,2) and is characterized by progressive memory loss and cognitive deterioration (1,3). Deposits of extracellular amyloid plaques made of amyloid- $\beta$  and neuronal intracellular neurofibrillary tangles (NFTs) composed of the protein tau are the primary pathological manifestations of AD (4).

AD can be divided into six stages, called Braak stages, based on the site of the tangle-bearing neurons and the rigorousness of modifications. The stages are defined as follows: I–II (transentorhinal stages), clinically silent cases; III–IV (limbic stage), incipient AD; and V–VI (neocortical stages), fully developed AD (3,5). The mini-mental state examination (MMSE) is a cognitive test used to screen and monitor dementia progression, such as that found in AD. It has been reported that a score below 24 of a possible 30 is indicative of dementia (6), and non-demented elderly patients usually score outside this range at 24 or above. The NFT scoring system is another related measure that is usually in accordance with Braak stages, with NFT III stage being indicative of AD (7).

Many researchers have found comprehensive evidence of the molecular pathogenesis of AD, and this information has been converted into promising treatment approaches, including immunotherapy using amyloid -  $\beta$ , which is being tested clinically (8). To understand the biology of AD and to provide measures of relevant pathophysiology in living individuals, biomarkers are becoming increasingly important in both AD patients and pre-symptomatic individuals. For AD patients, the biomarkers in the cerebrospinal fluid (CSF) are divided into basic and core biomarkers (9). Basic biomarkers comprise assays for blood-brain barrier (BBB) status and inflammatory methods, which have been developed to recognize disorders that may mimic or coincide with AD, for example, neuroborreliosis. Meanwhile, core biomarkers are used to recognize the chief pathogenic progressions of AD patients, and mainly reflect NFT and amyloid pathology, or axonal degeneration, such as  $A\beta_{1-42}$  (10,11), total tau levels (12,13), and phosphorylated tau levels (phosphorylated at thr181 or thr231) (14,15). Apart from  $a\beta$  and tau, many other novel candidate biomarkers have been recognized for CSF biomarkers (16). These included  $\beta$ site APP cleaving enzyme 1 (BACE1), which is the chief enzyme accountable for  $\beta$ -secretase activity; amyloid- $\beta$  oligomers, the accumulation of which

can form insoluble fibrillar  $A\beta$  in plaques; truncated amyloid- $\beta$  isoforms, the most available  $a\beta$  isoform in the CSF; and neuronal and synaptic markers, such as visinin-like protein 1, synaptotagmin, and growth-associated protein (9). It has been a challenge for independent studies to confirm the role of biomarkers in AD in peripheral blood; however, numerous candidate blood biomarkers have been anticipated.

Traditional studies of the mechanisms and biomarkers of AD predominantly emphasize a single gene or a specific pathway. However, the growth and advancement of AD is a complex process that is controlled by the accumulative impact of a sequence of genes and their interrelations.

As per the theory that genes with an analogous expression pattern might have same functions or take part in common cascades (17), the weighted gene co-expression network analysis (WGCNA) has emerged as an active approach for understanding the associations among diverse gene sets or among gene sets and clinical features (18,19). WGCNA has been extensively utilized in finding the hub genes related to the clinical features of various diseases (20–22).

In this study, WGCNA was implemented to conjointly examine clinical evidence and microarray records of AD patients' samples for the purpose of recognizing vital genes related to medical features. These vital genes may have essential clinical implications and be informative as investigative and predictive biomarkers or treatment targets. Finally, one of the hub genes, glutamate ionotropic receptor kainate type subunit 1 (*GRIK1*), was validated by an animal AD model, with the results showing that the mRNA and protein level of *GRIK1* in the AD hippocampus was increased compared with control (NC) hippocampus. Phalloidin staining showed that dendritic length of *GRIK1* pCDNA3.1 group was shorter than the NC group.

## Methods

### Data collection and preprocessing

Two expression profile data sets of AD were acquired from the Gene Expression Omnibus (GEO) database. Datasets GSE1297 and GSE28146, which focus on critical early stages, were chosen for further study (23,24). The GSE1297 dataset was utilized for AD-correlated modules and gene selection. Another dataset was used for independent verification.

Probes were mapped to gene symbols. Probes with more than one gene and empty probes were removed as

per the annotation platform of each expression profile. If there were numerous probes, which mapped to the similar gene symbol, their mean value was regarded as the gene manifestation value. Consequently, 12,502 unique genes representing the expression profiles of GSE1297, and 20846 unique genes representing GSE28146, were used for analysis.

In addition, as a common challenge in examining genome-wide expression data is managing batch effects, it is necessary to continuously monitor for batch effects whenever entirely analogous processing of samples is impossible. These data were normalized by means of the `normalizeBetweenArrays()` function in the `limma` library in R. After screening out the genes with the highest median absolute deviation (MAD) of 75%, 9,974 genes remained from GSE1297.

### Co-expression module detection

The `hclust()` function in the `stats` library in the R was used to perform cluster analysis of the samples with the suitable threshold value to both identify and eliminate the outliers. The gradient method was utilized to examine the independence and the average degree of connectivity of the numerous modules with diverse power values (the power values oscillated from 1 to 30). Once the suitable power value had been recognized when the degree of independence was 0.85, the module creation continued with the WGCNA process. Module identification was achieved by means of the dynamic tree cut method. The least number of genes was fixed at 30 to confirm greater dependability. Successively, the information relating to the analogous genes in each module was obtained.

### Module and clinical trait association analysis

The WGCNA algorithm uses module eigengenes (MEs) to evaluate the possible relationship of gene modules with clinical traits. MEs were defined as the primary key constituents computed by means of principal component analysis that recapitulates the manifestation of genes of a specific module into a single characteristic expression profile. The manifestation configurations of modules related to the types of samples were quantified by gene significance (GS) and module significance (MS). The GS measure was defined as the value of the Pearson correlation among the  $i$ -th gene profile  $x_i$  and the sample trait  $T$ :

$$GS_i = |\text{cor}(x_i, T)| \quad [1]$$

MS was defined as the average GS for all the genes in the module.

### Gene ontology (GO) and pathway enrichment analyses

The GO enrichment analyses of concerned gene sets were accomplished by means of DAVID (25).

### Association analysis and hub genes

The ME-based connectivity measure ( $k_{me}$ ) is the distance from the expression profile of a gene to that of the ME. The ME provides upsurge to a measure of module centrality ( $k_{me}$ ) as mentioned below:

$$k_{me}(i) = |\text{cor}(x(i), ME(q))| \quad [2]$$

$x(i)$  is the profile of gene  $i$  and  $ME(q)$  is the ME of module  $q$ . Therefore,  $k_{me}$  computes how adjacent a gene is to a module; i.e., it assesses the module membership of a gene. The hub genes are the ones with extensive network connectivity in a specific group. Moreover, the hub genes of modules are also largely related to the analogous clinical traits of the modules. Hence, genes with a high  $k_{me}$  in the module were casually denoted as intramodular hub genes in this study.

### Efficacy evaluation

Receiver operating characteristic (ROC) curve analysis was used to investigate the value of hub genes in diagnostic efficiency to differentiate among severe and non-severe AD patients. Detailed information of patients was obtained from a description of the GSE28146 dataset. The result was confirmed by the GSE28146 validation set. To do this, logistic regression was employed to classify the samples as follows:

$$p = 1 / \left( 1 + e^{-(\beta_0 + \beta_1 X_1 + \dots + \beta_k X_k)} \right) \quad [3]$$

Where  $p$  is the probability of severe stage,  $\beta_0 \dots \beta_k$  are the parameters to be estimated, and  $k$  is number of genes in a given module.

ROC curve was schemed, and the area under the curve (AUC) was quantified with "ROCR" package (Sing T, *et al.*, 2005; *Bioinformatics*). When an AUC value was higher than 0.7, the hub gene was regarded as having outstanding specificity and sensitivity. The outcome was established by the GSE28146 validation set.

### Animals

The AD mice and wild type (WT) mice we used were bought from Charles River (China). Briefly, the human mutant amyloid precursor protein (APP) (HuAPP<sup>sw</sup>) (Tg2576) transgenic mouse AD model was used. Animal experiments were conducted in accordance with the guideline for the Care and Use of Laboratory Animals published by the US National Institutes of Health.

Total RNA extraction and quantitative real-time reverse transcription polymerase chain reaction (qRT-PCR) analysis

Total RNA was isolated from AD mice and WT littermates (NC) using TRIzol reagent (Invitrogen) according to the manufacturer's protocol. The RNA of the cortex and hippocampus was isolated separately from the two groups. qRT-PCR was employed to determine the mRNA expression of *GRLK1*. qRT-PCR was performed using SYBRGreen qPCR Master Mix (TAKARA). The primer sequences are as follows: *GRIK1* forward: 5-CCGGAATTCCATGTTTTGTGATAGTTTTGCA-3, *GRIK1* reverse: 5-GAGTTCCTCGAGTCAGCTATGGTTTTGATCTT-3;  $\beta$ -actin forward: 5-CCCATCTATGAGGGTTACGC-3,  $\beta$ -actin reverse: 5-TTTAATGTCACGCACGATTTTC-3.

### Western blot analysis

Tissue was extracted using cell lysis buffer followed by immunoblotting with anti-GRIK1 (Abcam) and anti- $\beta$ -actin (Santa Cruz Biotechnology). Cells were lysed in RIPA buffer with protease inhibitors (Roche Applied Science) on ice for 20 min and then centrifuged at 13,500 rpm for 20 min at 4 °C. The supernatant was placed into a new tube, and the protein concentration was measured using the bicinchoninic acid protein assay kit (Applygen). Next, 30  $\mu$ g of cell lysates were resolved with 12.5% sodium dodecyl sulfate polyacrylamide gel electrophoresis and transferred to nitrocellulose membranes. Then, the membranes were blocked with 5% skim milk for 1 h at room temperature (RT). After blocking, the membranes were incubated with primary antibody for 1 h at RT. Then, the membranes were incubated with secondary antibodies at RT for 1 h. The protein bands were visualized using enhanced chemiluminescence chromogenic substrate with horseradish peroxidase (Beijing, China).

### Primary neuron culture

Primary neurons were isolated from the hippocampus of neonatal mice (26). Briefly, the extracted hippocampus was digested in 0.25% trypsin for 20 min. Cells were collected by centrifugation at 200  $\times$ g for 5 min. Isolated cells were cultured and maintained in Neurobasal<sup>TM</sup> medium (GIBCO) supplemented with B27 and L-glutamine (GIBCO).

### Cell transfection

The sequence of *GRIK1* used human liver cDNA (Invitrogen) and was cloned into the pCDNA3.1 vector (*GRIK1* pCDNA3.1). Primary neurons were seeded into a six-well plate at a concentration of  $10^5$ , and the plasmids or its control plasmids were transfected using Lipofectamine 2000 (Invitrogen), according to the manufacturer's protocols.

### Phalloidin staining

Primary neurons were fixed in 4% PFA for 20 min, permeabilized using 0.5% Triton X-100 (Biosharp, China) for 30 min, and treated with Alexa Fluor<sup>®</sup> 488 conjugated phalloidin (Cell Signaling, USA) for 30 min and the nuclear counterstain DAPI for 5 min. Coverslips were washed and mounted on glass slides. Stained neurons were photographed using a Nikon C2si confocal microscope (Nikon) equipped with a 60 $\times$  oil immersion objective.

## Results

### Identification of gene co-expression modules

To determine if all 31 samples in GSE1297 were appropriate for network analysis, the sample dendrogram and analogous clinical traits were investigated. We confirmed that all samples were incorporated into the groups and conceded the cutoff thresholds (*Figure 1A*). Soft-thresholding power is a crucial factor for creating a WGCNA. We accomplished the analysis of network topology for thresholding powers from 1 to 20. *Figure 1A,B,C* demonstrate that when the power value was equivalent to 6 (scale-free  $R^2 = 0.872$ ), our records projected a gene co-expression network that displayed scale-free topology with integral modular features.

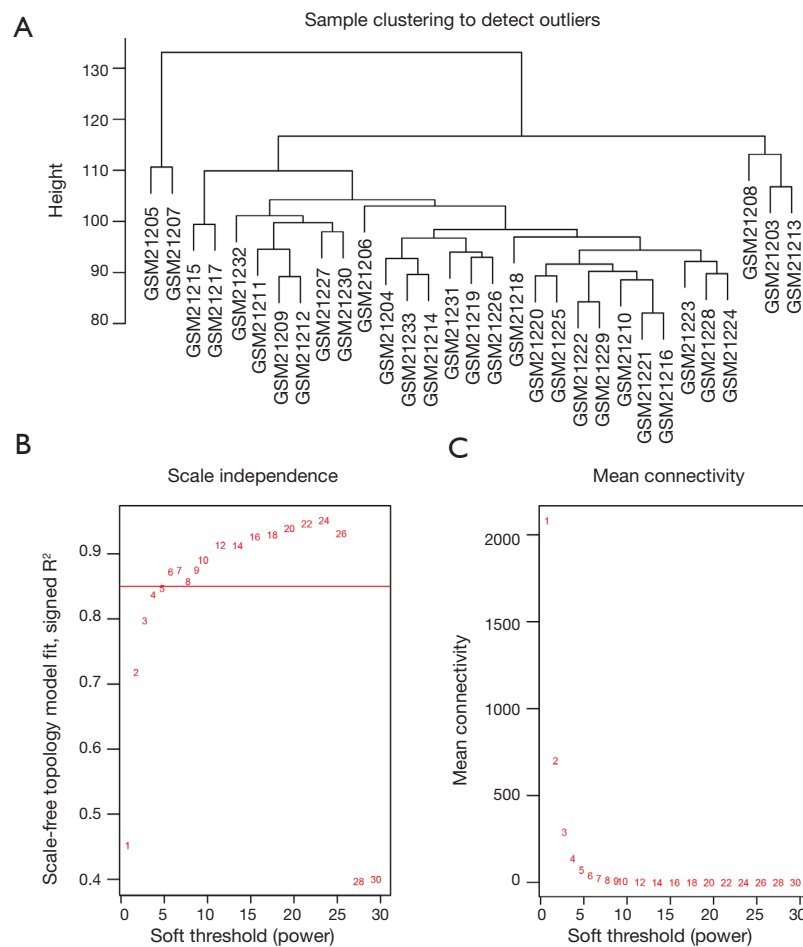


**Figure 1** Clustering of samples and detection of soft-thresholding power. (A) Sample clustering was conducted to detect outliers. All samples are situated in the clusters and passed the cutoff thresholds; (B,C) analysis of the scale-free fit index (B) and analysis of the mean connectivity (C) for numerous soft-thresholding powers.

Finally, we created average linkage hierarchical clustering with the topological overlap matrix (TOM) and created the gene co-expression network by means of WGCNA depending on the graded grouping of the quantified variations. Subsequently, 16 modules were acquired (Figure 2). We utilized MEs as illustrative profiles and computed module correspondence by eigengene correlation. Interaction relations of the 16 modules were examined, and the network heatmap was designed (Figure 3A). The outcomes indicated that each module was autonomously authenticated with another which revealed a high level of individuality among the modules and the comparative independence of gene manifestation in each module.

### Correlation of modules and clinical traits

To investigate if any module was connected with disease status, we investigated the relevance among each module plus the AD clinical traits, including MMSE, BRAAK, NFT, postmortem interval (PMI), and age. We found that some modules were highly correlated with the disease status of AD (modules of lightcyan, pink, salmon, and blue). For example, the ME value of the lightcyan module also exhibited a positive association with MMSE ( $r=0.6$ ,  $P=3 \times 10^{-4}$ ) and a negative association with BRAAK ( $r=-0.41$ ,  $P=0.02$ ) (Figure 3B). The eigengene dendrogram and the heatmap specified that the 16 modules



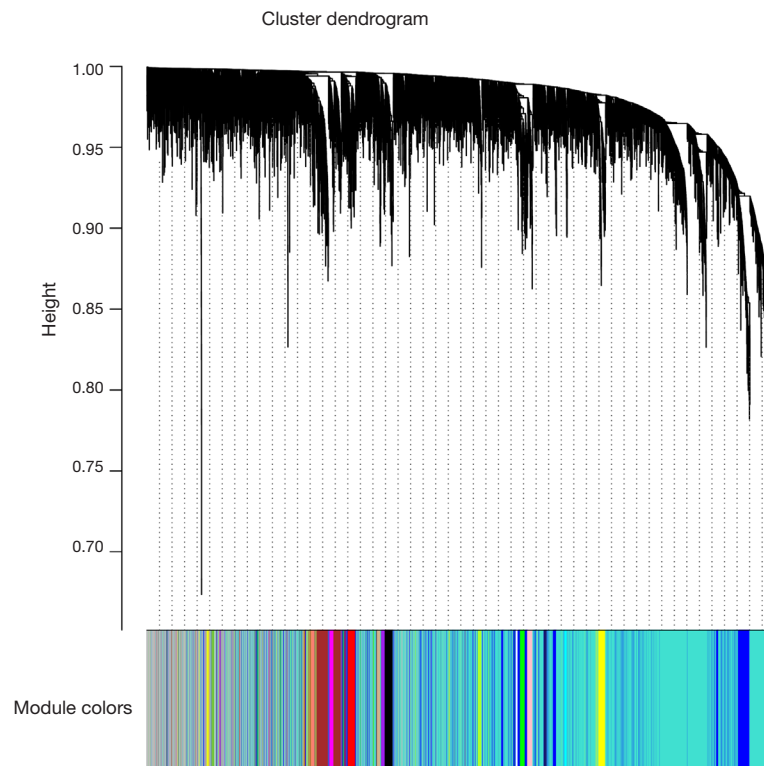


**Figure 2** Dendrogram of all genes grouped depending on a dissimilarity measure (1-TOM). TOM, topological overlap matrix.

were mostly separated into two groups (*Figure 3C*). Moreover, the ME of the pink module indicated a significant connection with all disease status (NFT, BRAAK, and MMSE) compare to the other modules (*Figure 3B*), indicating that the pink module might have an integral role in the occurrence and development of AD. We recognized the pink module as the module most applicable to the disease level of AD. Finally, a correlation between module membership and GS was plotted for the module pink (*Figure 4A,B,C*). We visualized the pink module as a network in Cytoscape. *Figure 4D* shows the genes in the pink module, and the red nodes signify hub genes. The hub genes in the pink module comprised acetoacetyl-CoA synthetase (*AACS*), *GRIK1*, homeobox B2 (*HOXB2*), potassium voltage-gated channel modifier subfamily F member 1 (*KCNF1*), MYB proto-oncogene like 1 (*MYBL1*), and RAP1 GTPase activating protein 2 (*RAP1GAP2*).

#### **Functional enrichment analysis of genes in modules of interest**

Since genes with analogous expression patterns might

take part in parallel biological procedures or networks, we achieved enrichment analysis to search the GO terms in which the pink module was incorporated. As per the obtained outcomes, the pink module was mostly enriched in central nervous system development, regulation of phosphatidylinositol 3-kinase (PI3K) signaling, and ion transmembrane transport (*Figure 4E & Table 1*). To further investigate the role of modules in AD, we also performed GO enrichment analysis to other modules, which were correlated with two of three clinical traits (modules of lightcyan, salmon, and blue). Interestingly, the genes in the blue, salmon and pink modules were significantly enriched in the GO terms of the plasma membrane (*Figure S1*).

#### **Efficacy evaluation of hub genes**

In the GSE28146 validation set, we found that genes in the pink module are capable of discriminating severe and non-severe AD samples (*Figure 5A*). Furthermore, ROC curve analysis was executed to assess the diagnostic effectiveness of hub genes to differentiate among severe and non-severe AD samples. We quantified the AUC value and designed ROC

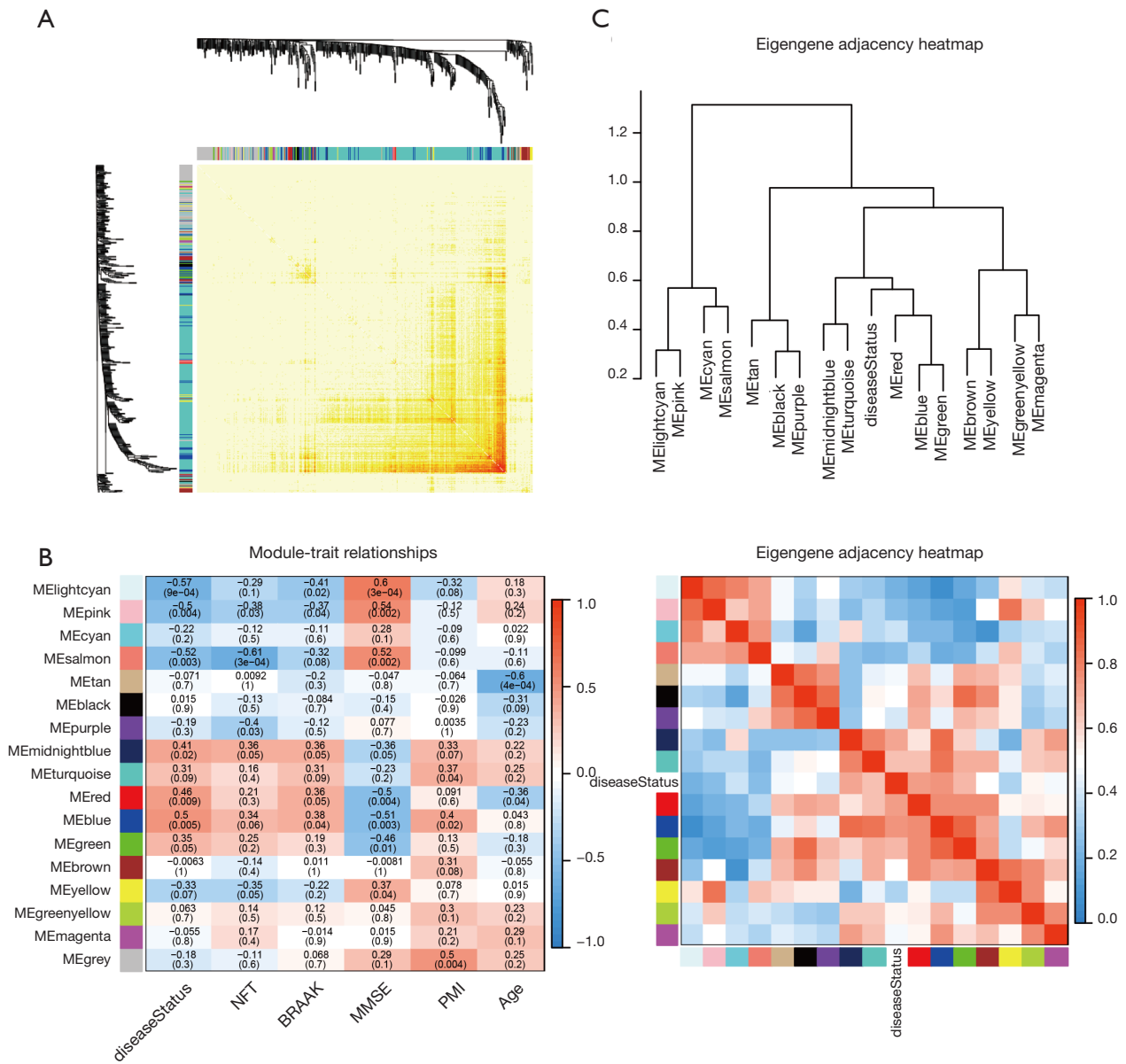


**Figure 3** Identification of modules associated with the clinical traits of AD. (A) A heatmap of co-expressed genes. Different colors in the X and Y axis signify different modules. The intensity of yellow represents the degree of connectivity of different modules; (B) correlation among modules and traits; (C) top: dendrogram of ME acquired by WGCNA; bottom: heatmap plot of the adjacencies of modules. Red represents high adjacency whereas blue represents low adjacency. AD, Alzheimer’s disease; ME, module eigengene; NFT, neurofibrillary tangle; MMSE, mini-mental state examination; PMI, postmortem interval; WGCNA, weighted gene co-expression network analysis.

curves for the six hub genes. The AUC value of the pink module was greater than 0.7 (Figure 5B). The ROC curves for hub genes of the other less related modules (modules of lightcyan, salmon, and blue) are presented in Figure S2.

*GRIK1 was upregulated in the AD cortex and AD hippocampus and attenuated dendritic length in primary neurons*

To identify the levels of *GRIK1* in the AD cortex and AD

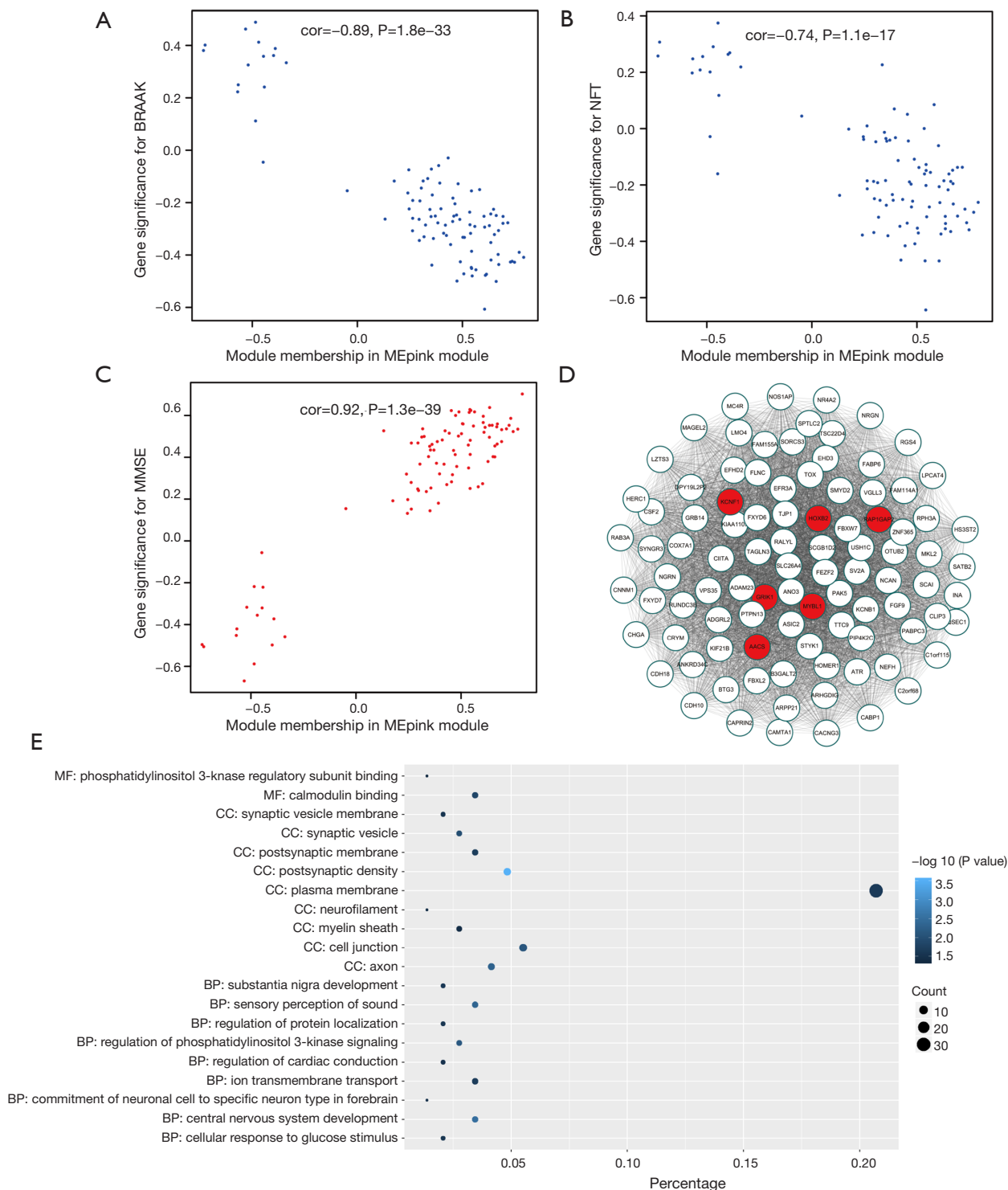


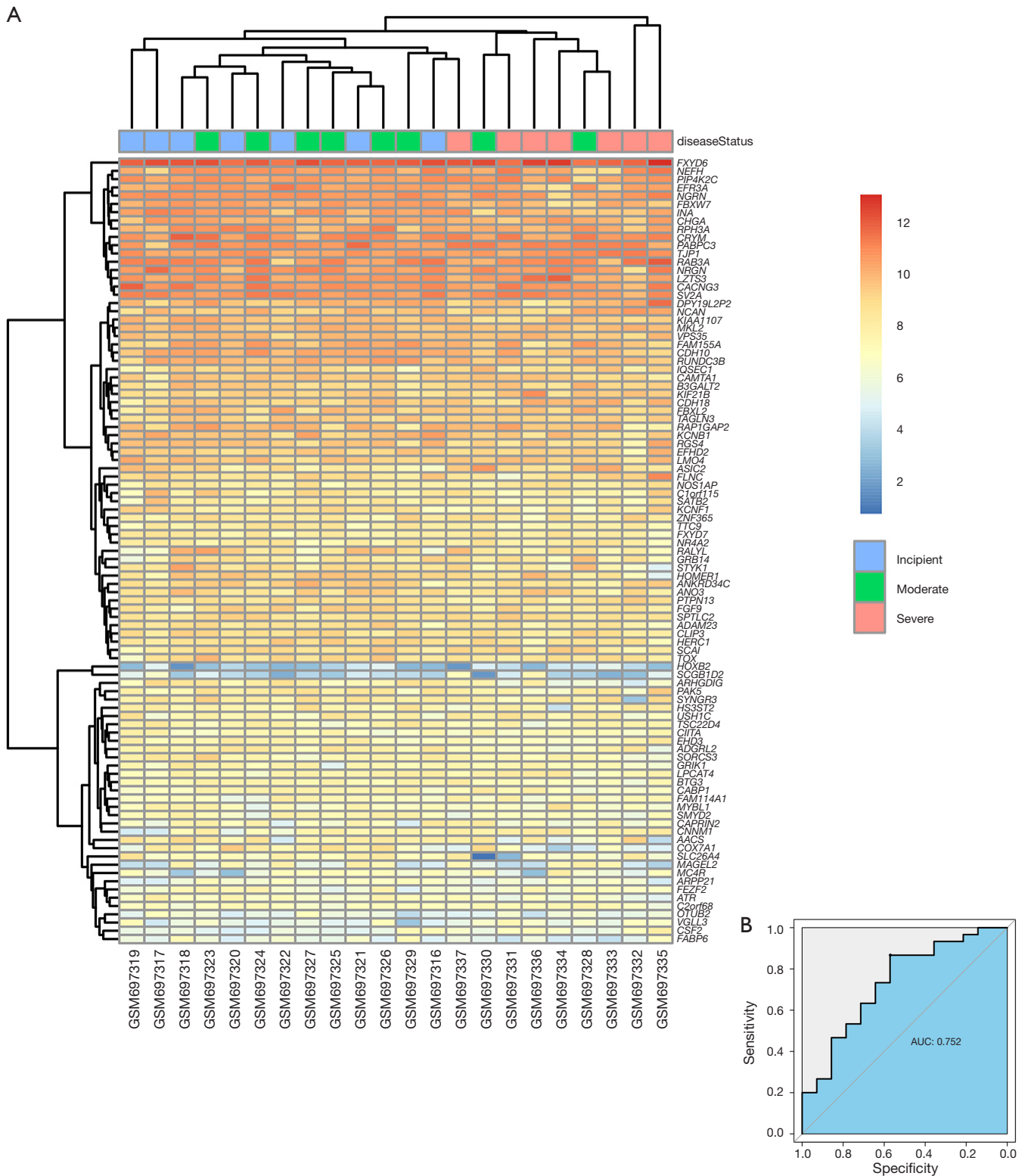
**Figure 4** Clinical relevance and functional analysis of genes in module Mepink. (A,B,C) A scatter plot of gene significance for NFT (A), BRAAK (B), and MMSE (C) vs. the module membership in the pink module; (D) the genes in the pink module and the red signify the hub nodes; (E) statistics of GO term enrichment for genes in different modules for WGCNA. Percentage is the ratio of the number of genes of a specific module in a certain pathway to the number of total genes. ME, module eigengene; NFT, neurofibrillary tangle; MMSE, mini-mental state examination; GO, gene ontology; WGCNA, weighted gene co-expression network analysis.



**Table 1** Enriched GO terms of the pink module

Term	P value	Genes
Central nervous system development	0.003082	<i>GRIK1, ADAM23, ASIC2, NCAN, TAGLN3</i>
Sensory perception of sound	0.004451	<i>SLC26A4, TJP1, ASIC2, USH1C, CRYM</i>
Regulation of phosphatidylinositol 3-kinase signaling	0.007014	<i>FGF9, PTPN13, PIP4K2C, FBXL2</i>
Ion transmembrane transport	0.021093	<i>GRIK1, ANO3, ASIC2, FXYD6, FXYD7</i>
Substantia nigra development	0.02498	<i>INA, FGF9, SYNGR3</i>
Regulation of protein localization	0.027896	<i>SLC26A4, ARHGDIG, FBXW7</i>
Cellular response to glucose stimulus	0.027896	<i>TJP1, KCNB1, AACS</i>
Regulation of cardiac conduction	0.031987	<i>FXYD6, EHD3, FXYD7</i>
Commitment of neuronal cell to specific neuron type in forebrain	0.034502	<i>FEZF2, SATB2</i>
Positive regulation of GTPase activity	0.063638	<i>CSF2, ARHGDIG, FGF9, RGS4, HERC1, RAP1GAP2, IQSEC1</i>
Negative regulation of transcription from RNA polymerase II promoter	0.068575	<i>CIITA, FEZF2, SATB2, FGF9, NR4A2, SMYD2, TAGLN3, CRYM</i>
Glutamate receptor signaling pathway	0.072494	<i>GRIK1, KCNB1</i>
Phosphatidylinositol phosphorylation	0.080478	<i>FGF9, EFR3A, PIP4K2C</i>
Postsynaptic density	3.01E-04	<i>LZTS3, CABP1, NEFH, VPS35, NRGN, HOMER1, SORCS3</i>
Axon	0.004873	<i>RAB3A, KCNB1, NEFH, NRGN, HOMER1, KIF21B</i>
Cell junction	0.007625	<i>LZTS3, TJP1, GRIK1, KCNB1, CABP1, RPH3A, HOMER1, SYNGR3</i>
Synaptic vesicle	0.01066	<i>RAB3A, SV2A, RPH3A, SYNGR3</i>
Postsynaptic membrane	0.020603	<i>LZTS3, GRIK1, KCNB1, CABP1, HOMER1</i>
Plasma membrane	0.022859	<i>RAB3A, GRIK1, CABP1, FXYD6, FXYD7, SORCS3, ANO3, EFR3A, SV2A, RAP1GAP2, ADAM23, KCNB1, ASIC2, PTPN13, CACNG3, RPH3A, FLNC, CNNM1, SLC26A4, STYK1, TJP1, RGS4, CDH18, MC4R, USH1C, FAM155A, KCNF1, CLIP3, GRB14, CDH10</i>
Synaptic vesicle membrane	0.03024	<i>SV2A, RPH3A, SYNGR3</i>
Neurofilament	0.038839	<i>INA, NEFH</i>
Myelin sheath	0.039486	<i>INA, NEFH, TAGLN3, EHD3</i>
Apical part of cell	0.053059	<i>TJP1, USH1C, HOMER1</i>
Cytoplasm	0.06079	<i>LZTS3, CAMTA1, ARHGDIG, ARPP21, FGF9, ZNF365, FBXW7, TSC22D4, PAK5, PABPC3, NEFH, SV2A, RAP1GAP2, KIF21B, EHD3, IQSEC1, SATB2, NR4A2, SCAI, PTPN13, SMYD2, HERC1, FLNC, CAPRIN2, TJP1, FAM114A1, HOXB2, RGS4, BTG3, USH1C, GRB14, CRYM, FABP6, FBXL2</i>
Sarcolemma	0.066156	<i>NOS1AP, KCNB1, FLNC</i>
Costamere	0.089819	<i>FLNC, HOMER1</i>
Calmodulin binding	0.014081	<i>TJP1, ARPP21, RGS4, NRGN, FBXL2</i>
Phosphatidylinositol 3-kinase regulatory subunit binding	0.043401	<i>PTPN13, FBXL2</i>

GO, gene ontology.



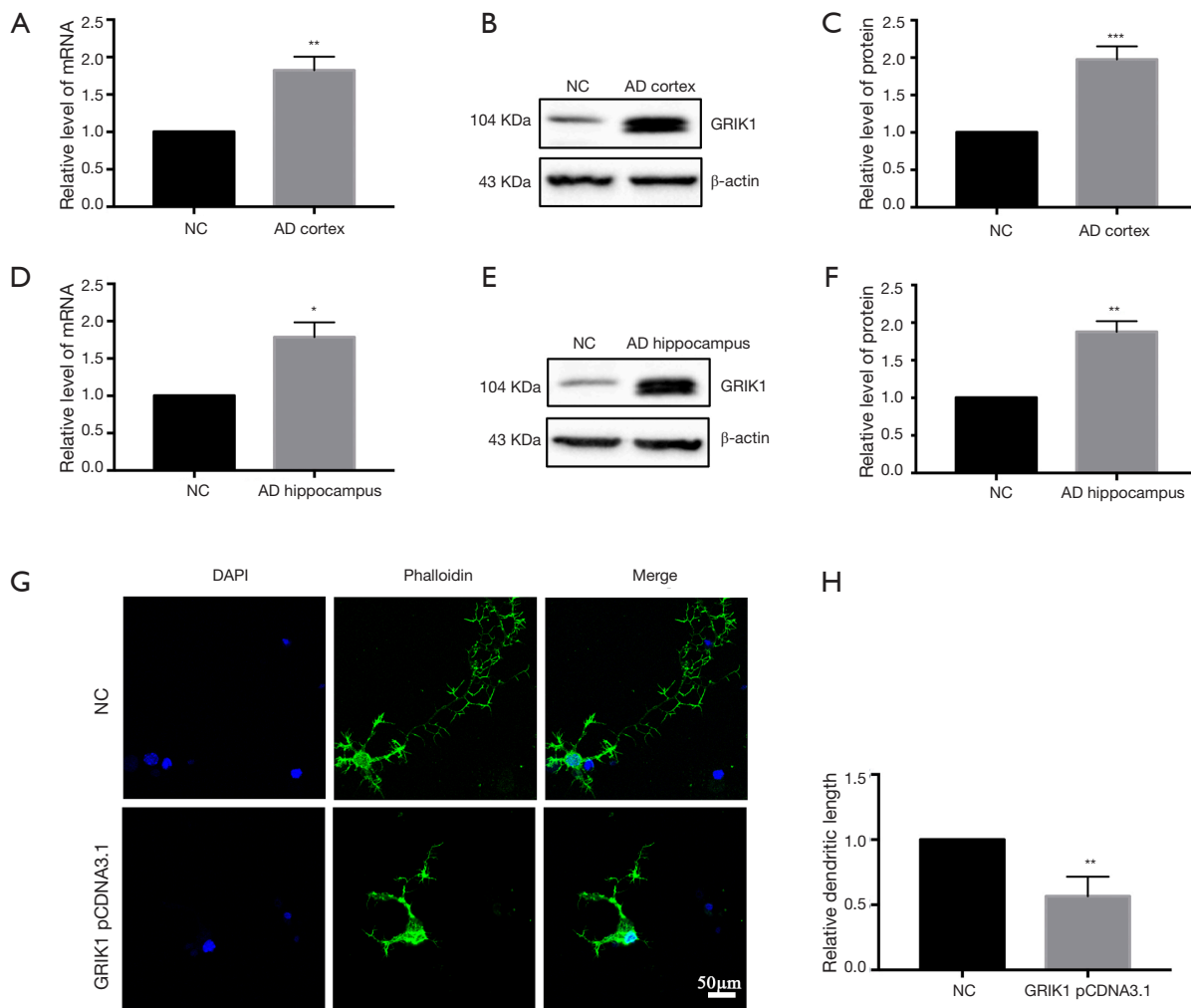


**Figure 6** The expression of GRIK1 in the AD cortex and AD hippocampus. (A) The expression of GRIK1 in the AD cortex determined by qRT-PCR. \*\*,  $P < 0.01$ . NC: The control group,  $n = 10$ ; the AD group,  $n = 10$ ; (B) Western blot showing the expression of GRIK1 in the AD cortex and control group; (C) relative expression of GRIK1 in (B). \*\*\*,  $P < 0.005$ .  $n = 3$ ; (D) the expression of GRIK1 in the AD hippocampus determined by qRT-PCR. \*,  $P < 0.05$ , NC: the control group,  $n = 10$ ; the AD group,  $n = 10$ ; (E) Western blot showing the expression of GRIK1 in the AD hippocampus and control group; (F) relative expression of GRIK1 in (E). \*\*,  $P < 0.01$ .  $n = 3$ ; (G) phalloidin staining showing the morphology of the primary neurons; (H) relative dendritic length in (G). \*\*,  $P < 0.01$ .  $n = 3$ . The experiments were independently repeated 3 times. AD, Alzheimer's disease; qRT-PCR, quantitative real-time reverse transcription polymerase chain reaction.

hippocampus, qRT-PCR and western blot were used. The qRT-PCR data showed that the mRNA level of *GRIK1* was higher in the AD cortex compared with the NC cortex (Figure 6A). Western blotting data showed that the expression of *GRIK1* protein was higher in the AD cortex compared to the NC cortex (Figure 6B,C). A comparison of the expression of *GRIK1* between the AD hippocampus and NC hippocampus was also examined via qRT-PCR

and Western blot. The mRNA level of *GRIK1* in the AD hippocampus was increased compared with the NC hippocampus (Figure 6D). The protein level of *GRIK1* in the AD hippocampus showed the same pattern (Figure 6E,F). Phalloidin staining showed that the dendritic length of *GRIK1* pCDNA3.1 group was shorter than that in the NC group (Figure 6G,H), These data indicated that *GRIK1* was upregulated both in the AD cortex and AD hippocampus

and attenuated the dendritic length of primary neurons.

## Discussion

This study combined the mining of microarray data with the clinical evidence of AD patients to perform a WGCNA with the aim of recognizing those biomarkers related to clinical features that could distinguish the different stages of AD patients.

There are many different stage standards for differentiating AD types. Based on the foundation of the dispersal of NFTs, AD can be divided into three subtypes (Braak stage  $\geq$  IV): hippocampal-sparing AD, typical AD, and limbic-predominant AD. In hippocampal-sparing AD, NFTs are increased in the cortex but relatively less so in the hippocampus (27). However, in limbic-predominant AD, NFT counts are normally increased in the hippocampus and decreased in the cortex. Meanwhile, typical AD usually has classic distributions of NFTs (28). According to neuroimaging patterns of CSF biomarkers, cognitive and clinical measures, white matter hyperintensities, and longitudinal trajectories, AD can be divided into four atrophy patterns: (I) patients with generally standard neuroanatomical profiles with slightly irregular cognitive and CSF biomarker profiles and the slowest clinical development; (II) patients with classical AD neuroanatomical, cognitive, and CSF biomarkers with a clinical profile displaying the quickest clinical development; (III) patients with a diffused array of deterioration with comparatively less distinct participation of the medial temporal lobe, irregular CSF amyloid- $\beta$ 1-42 values, and proportionately superior executive damage; (IV) patients with remarkably central participation of the medial temporal lobe and a slow stable development, possibly demonstrating in early AD stages (5). These biomarkers for staging AD offer the prospect for allowing accurate diagnosis, prognosis, and precise patient enrolment of comparatively consistent subgroups of individuals for clinical trials.

In this study, the GSE1297 and GSE28146 datasets, which focused on the critical early stages, were chosen for further study. GSE1297 dataset was utilized for AD-related modules and gene selection. Another dataset was used for independent verification. After some processes such as standardization and normalization, 9,974 genes were finally used for WGCNA. Then, 16 co-expression modules were recognized by the dynamic tree cut method. Through associating gene modules with three clinical features, the pink module was identified as having the greatest positive

association with the pathological stage. Exploring the association between the pink module and pathological stage could narrow the search for those genes with vital biological importance to AD. There were six hub genes in the pink module, including *AACS*, *GRIK1*, *HOXB2*, *KCNF1*, *MYBL1*, and *RAP1GAP2*. Of these hub genes, mutations in the *PSEN1* gene have been found to be linked with familial AD (29). The transcriptional factor *HOXB2* has been proven to be up-regulated with folic acid to augment the effectiveness of memantine for spatial learning and neuronal defense (30). *MYBL1* has shown different patterns in males' and females' molecular networks of AD based on global gene expression and integrative network analyses (31). *Bos taurus* *RAP1GAP2* acts together with synaptotagmin-like protein 1 and Rab27 to control the excretion of dense granules from platelets at locations of endothelial injury, which may impact the progress of AD (32). *KCNF1* has diverse functions, including regulating neurotransmitter release and *AACS*-related pathways of metabolism and butanoate metabolism, which may play roles in AD (33).

*GRIK1*, also known as glutamate receptor 5 (*GluR5*), is one of 14 receptor subunits. The glutamate receptor (*GluR*) subunits are included in ionotropic *GluRs* and regulate excitatory neurotransmission (34). A physical map of the *GRIK1* region and a schematic representation of the splicing mechanisms were presented by Barbon *et al.* in 2000 (35). In 2014, Kranzler *et al.* showed that *GRIK1* could reduce the heavy drinking in problem drinkers and that it might be a moderator for heavy drinkers (36). The function of *GRIK1* in the central nervous system has not been fully characterized. *GRIK1* was shown to be overexpressed in senile plaques (in the temporal lobe) in RNA-sequencing data of AD patients and may play a critical role in AD (37). However, the relationship between AD and *GRIK1* is poorly understood. Therefore, we next investigated the level of *GRIK1* in a mouse model. The results showed that the expression of *GRIK1* was upregulated in both the cortex and hippocampus in AD mice, indicating a potential role in the pathogenesis of AD.

Enrichment analyses for the pink module specified that the biological processes of the pink module concentrated on PI3K signaling and ion transmembrane transport. Previous studies have suggested that the PI3K/Akt cascade is involved in the nicotine-induced neuroprotection through the phosphorylation of bad, a Bcl-2 family protein supporting neuronal endurance (38). Kihara *et al.* reported that nicotine treatment could promote the phosphorylation of Akt and the manifestation of Bcl-2 while protecting neurons from

b-amyloid-enhanced glutamate neurotoxicity. Treatment with PI3K inhibitors like LY294002 and wortmannin can suppress the nicotine-induced neuroprotective impact, indicating that the PI3K/Akt cascade regulates the nicotine-induced neuroprotection through the Bcl-2 protein (39). Donepezil, galantamine, tacrine, specified as “therapeutic AChE inhibitors” and used in the treatment of AD, were shown to protect the principal cultures of rat cortical neurons from glutamate-induced neurotoxicity that includes apoptotic neuronal death via PI3K/Akt pathway (40).

One of the pathological changes in AD is the irregular proteolytic handling of APP, which is the vital step that causes the creation of amyloid plaque, NFTs, and neuronal loss. By interacting with ion transport systems, amyloid protein induces an array of effects via the activation of several mechanisms (41). Impairment of  $Ca^{2+}$  homeostasis, along with the production of reactive oxygen species was considered as the cause of amyloid protein-prompted cytotoxicity. The change in  $Ca^{2+}$  homeostasis may change endogenous ion transport systems, like as  $Ca^{2+}$  and  $K^+$  channels, ligand-driven ion channels, and G-protein-induced releases of second messengers or form heterogeneous ion channels. Amyloid proteins in AD modify numerous ion transport systems and form heterogeneous ion channels, which can alter cell regulation (42). These modifications harm the membrane by lowering its reliability and increasing its ion penetrability, thus perhaps promoting the progress of AD (42).

Moreover, we found that genes in the pink module can be used to discriminate between three kinds of AD samples of the incipient, moderate, and severe type, particularly between severe and non-severe AD samples in the GSE28146 validation set. Furthermore, ROC curve analysis was applied to assess the diagnostic effectiveness of six hub genes to discriminate between severe and non-severe AD samples. We found that the AUC value was higher than 0.7, but that the AUC values for less related modules (modules of lightcyan, salmon, and blue) were lower than 0.7, indicating that these six hub genes are potential biomarkers of AD stages.

In conclusion, we employed WGCNA to systematically recognize co-expressed gene modules and those hub genes related to AD development. One gene module and six hub genes capable of distinguishing between AD stages were identified. These outcomes can contribute to an improved understanding of the mechanisms participating in the development of AD.

## Acknowledgments

None.

## Footnote

*Conflict of Interest:* The authors have no conflicts of interest to declare.

*Ethical Statement:* The authors are accountable for all aspects of the work in ensuring that questions related to the accuracy or integrity of any part of the work are appropriately investigated and resolved. Animal experiments were conducted in accordance with the guideline for the Care and Use of Laboratory Animals published by the US National Institutes of Health. The study was approved by the Ethics Committee of First Affiliated Hospital of Harbin Medical University, China (No. 2019022).

## References

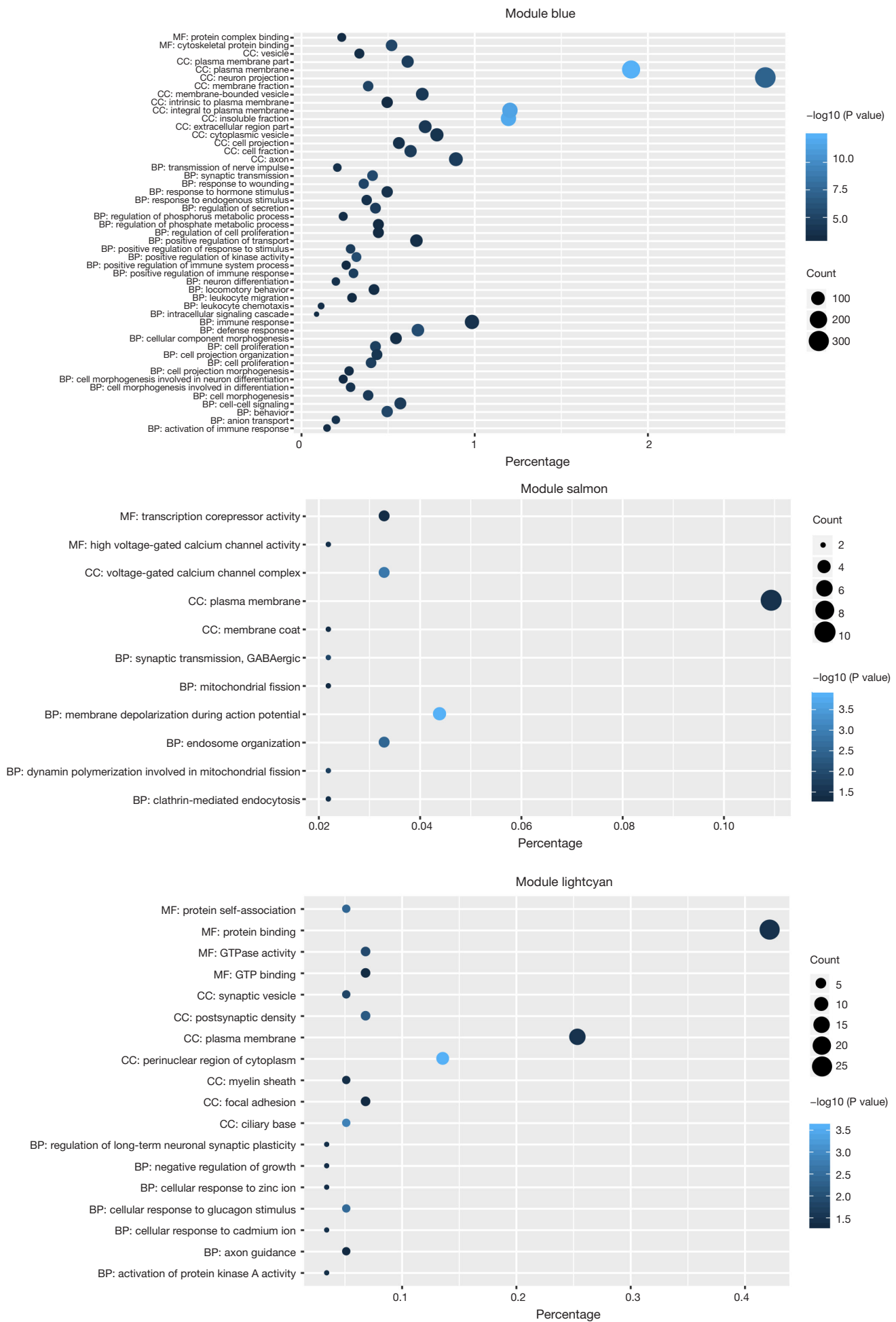
1. Albert MS, DeKosky ST, Dickson D, et al. The diagnosis of mild cognitive impairment due to Alzheimer's disease: recommendations from the National Institute on Aging-Alzheimer's Association workgroups on diagnostic guidelines for Alzheimer's disease. *Alzheimers Dement* 2011;7:270-9.
2. Vemuri P, Lesnick TG, Przybelski SA, et al. Effect of lifestyle activities on Alzheimer disease biomarkers and cognition. *Ann Neurol* 2012;72:730-8.
3. Sperling RA, Aisen PS, Beckett LA, et al. Toward defining the preclinical stages of Alzheimer's disease: recommendations from the National Institute on Aging-Alzheimer's Association workgroups on diagnostic guidelines for Alzheimer's disease. *Alzheimers Dement* 2011;7:280-92.
4. Mielke MM, Vemuri P, Rocca WA. Clinical epidemiology of Alzheimer's disease: assessing sex and gender differences. *Clin Epidemiol* 2014;6:37-48.
5. Braak H, Braak E. Staging of Alzheimer's disease-related neurofibrillary changes. *Neurobiol Aging* 1995;16:271-8; discussion 278-84.
6. Galasko D, Klauber MR, Hofstetter CR, et al. The Mini-Mental State Examination in the early diagnosis of Alzheimer's disease. *Arch Neurol* 1990;47:49-52.
7. Bierer LM, Hof PR, Purohit DP, et al. Neocortical neurofibrillary tangles correlate with dementia severity in



- Alzheimer's disease. *Arch Neurol* 1995;52:81-8.
8. Wang YQ, Qu DH, Wang K. Therapeutic approaches to Alzheimer's disease through stimulating of non-amyloidogenic processing of amyloid precursor protein. *Eur Rev Med Pharmacol Sci* 2016;20:2389-403.
  9. Blennow K, Hampel H, Weiner M, et al. Cerebrospinal fluid and plasma biomarkers in Alzheimer disease. *Nat Rev Neurol* 2010;6:131-44.
  10. Fagan AM, Mintun MA, Mach RH, et al. Inverse relation between in vivo amyloid imaging load and cerebrospinal fluid Abeta42 in humans. *Ann Neurol* 2006;59:512-9.
  11. Forsberg A, Engler H, Almkvist O, et al. PET imaging of amyloid deposition in patients with mild cognitive impairment. *Neurobiol Aging* 2008;29:1456-65.
  12. Hesse C, Rosengren L, Andreasen N, et al. Transient increase in total tau but not phospho-tau in human cerebrospinal fluid after acute stroke. *Neurosci Lett* 2001;297:187-90.
  13. Ost M, Nylen K, Csajbok L, et al. Initial CSF total tau correlates with 1-year outcome in patients with traumatic brain injury. *Neurology* 2006;67:1600-4.
  14. Hampel H, Burger K, Pruessner JC, et al. Correlation of cerebrospinal fluid levels of tau protein phosphorylated at threonine 231 with rates of hippocampal atrophy in Alzheimer disease. *Arch Neurol* 2005;62:770-3.
  15. Buerger K, Ewers M, Pirttila T, et al. CSF phosphorylated tau protein correlates with neocortical neurofibrillary pathology in Alzheimer's disease. *Brain* 2006;129:3035-41.
  16. Villemagne VL, Pike KE, Chetelat G, et al. Longitudinal assessment of Abeta and cognition in aging and Alzheimer disease. *Ann Neurol* 2011;69:181-92.
  17. Carlson MR, Zhang B, Fang Z, et al. Gene connectivity, function, and sequence conservation: predictions from modular yeast co-expression networks. *BMC Genomics* 2006;7:40.
  18. Zhou XG, Huang XL, Liang SY, et al. Identifying miRNA and gene modules of colon cancer associated with pathological stage by weighted gene co-expression network analysis. *Onco Targets Ther* 2018;11:2815-30.
  19. Langfelder P, Horvath S. WGCNA: an R package for weighted correlation network analysis. *BMC Bioinformatics* 2008;9:559.
  20. Liu J, Zhou S, Li S, et al. Eleven genes associated with progression and prognosis of endometrial cancer (EC) identified by comprehensive bioinformatics analysis. *Cancer Cell Int* 2019;19:136.
  21. Zhao B, Chen Y, Hu S, et al. Systematic Analysis of Non-coding RNAs Involved in the Angora Rabbit (*Oryctolagus cuniculus*) Hair Follicle Cycle by RNA Sequencing. *Front Genet* 2019;10:407.
  22. Parsana P, Ruberman C, Jaffe AE, et al. Addressing confounding artifacts in reconstruction of gene co-expression networks. *Genome Biol* 2019;20:94.
  23. Blalock EM, Geddes JW, Chen KC, et al. Incipient Alzheimer's disease: microarray correlation analyses reveal major transcriptional and tumor suppressor responses. *Proc Natl Acad Sci U S A* 2004;101:2173-8.
  24. Blalock EM, Buechel HM, Popovic J, et al. Microarray analyses of laser-captured hippocampus reveal distinct gray and white matter signatures associated with incipient Alzheimer's disease. *J Chem Neuroanat* 2011;42:118-26.
  25. Huang DW, Sherman BT, Tan Q, et al. DAVID Bioinformatics Resources: expanded annotation database and novel algorithms to better extract biology from large gene lists. *Nucleic Acids Res* 2007;35:W169-75.
  26. Si Z, Wang X, Zhang Z, et al. Heme Oxygenase 1 Induces Tau Oligomer Formation and Synapse Aberrations in Hippocampal Neurons. *J Alzheimers Dis* 2018;65:409-19.
  27. Murray ME, Graff-Radford NR, Ross OA, et al. Neuropathologically defined subtypes of Alzheimer's disease with distinct clinical characteristics: a retrospective study. *Lancet Neurol* 2011;10:785-96.
  28. Whitwell JL, Dickson DW, Murray ME, et al. Neuroimaging correlates of pathologically defined subtypes of Alzheimer's disease: a case-control study. *Lancet Neurol* 2012;11:868-77.
  29. Antonell A, Llado A, Altirriba J, et al. A preliminary study of the whole-genome expression profile of sporadic and monogenic early-onset Alzheimer's disease. *Neurobiol Aging* 2013;34:1772-8.
  30. Chen TF, Huang RF, Lin SE, et al. Folic Acid potentiates the effect of memantine on spatial learning and neuronal protection in an Alzheimer's disease transgenic model. *J Alzheimers Dis* 2010;20:607-15.
  31. Sun LL, Yang SL, Sun H, et al. Molecular differences in Alzheimer's disease between male and female patients determined by integrative network analysis. *J Cell Mol Med* 2019;23:47-58.
  32. Willard FS, Low AB, McCudden CR, et al. Differential G-alpha interaction capacities of the GoLoco motifs in Rap GTPase activating proteins. *Cell Signal* 2007;19:428-38.
  33. Gutman GA, Chandy KG, Grissmer S, et al. International Union of Pharmacology. LIII. Nomenclature and molecular relationships of voltage-gated potassium channels. *Pharmacol Rev* 2005;57:473-508.
  34. Sommer B, Seeburg PH. Glutamate receptor channels:

- novel properties and new clones. *Trends Pharmacol Sci* 1992;13:291-6.
35. Barbon A, Barlati S. Genomic organization, proposed alternative splicing mechanisms, and RNA editing structure of GRIK1. *Cytogenet Cell Genet* 2000;88:236-9.
  36. Kranzler HR, Covault J, Feinn R, et al. Topiramate treatment for heavy drinkers: moderation by a GRIK1 polymorphism. *Am J Psychiatry* 2014;171:445-52.
  37. Twine NA, Janitz K, Wilkins MR, et al. Whole transcriptome sequencing reveals gene expression and splicing differences in brain regions affected by Alzheimer's disease. *PLoS One* 2011;6:e16266.
  38. del Peso L, Gonzalez-Garcia M, Page C, et al. Interleukin-3-induced phosphorylation of BAD through the protein kinase Akt. *Science* 1997;278:687-9.
  39. Kihara T, Shimohama S, Sawada H, et al. alpha 7 nicotinic receptor transduces signals to phosphatidylinositol 3-kinase to block A beta-amyloid-induced neurotoxicity. *J Biol Chem* 2001;276:13541-6.
  40. Takada-Takatori Y, Kume T, Sugimoto M, et al. Acetylcholinesterase inhibitors used in treatment of Alzheimer's disease prevent glutamate neurotoxicity via nicotinic acetylcholine receptors and phosphatidylinositol 3-kinase cascade. *Neuropharmacology* 2006;51:474-86.
  41. Sultana R, Newman SF, Abdul HM, et al. Protective effect of D609 against amyloid-beta1-42-induced oxidative modification of neuronal proteins: redox proteomics study. *J Neurosci Res* 2006;84:409-17.
  42. Casey NH, Crosley RI, Smith GA. Influence of continuous dietary halofuginone on broiler skin tensile strength and growth performance. *J S Afr Vet Assoc* 1992;63:16-9.

**Cite this article as:** Sun Y, Lin J, Zhang L. The application of weighted gene co-expression network analysis in identifying key modules and hub genes associated with disease status in Alzheimer's disease. *Ann Transl Med* 2019;7(24):800. doi: 10.21037/atm.2019.12.59



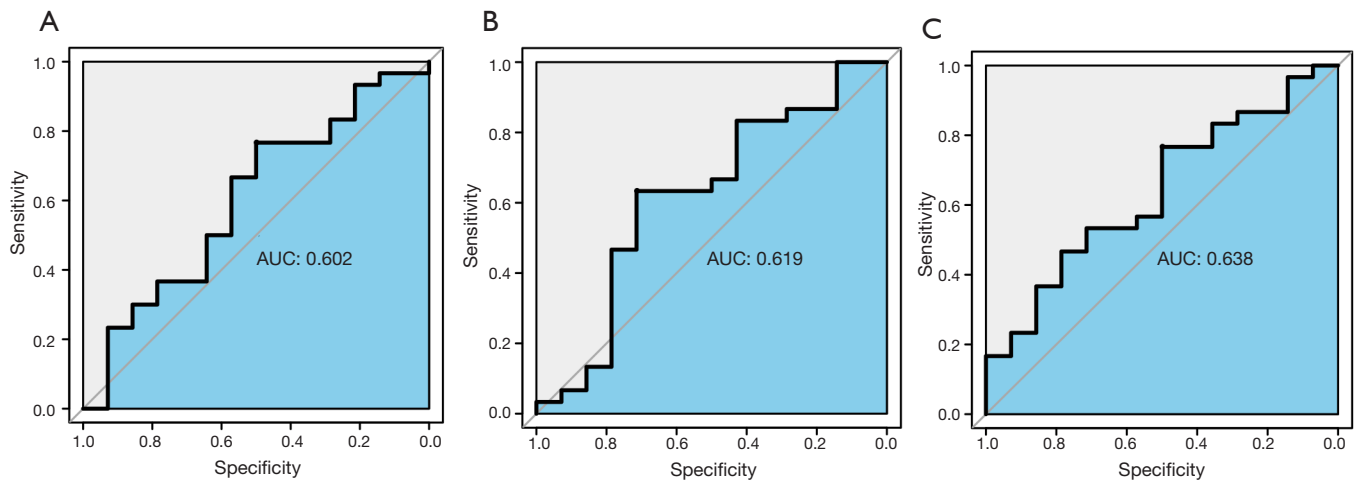


**Figure S2** ROC curve for the hub genes in blue (A), salmon (B), and lightcyan (C) modules. ROC, receiver operating characteristic; AUC, area under the curve.